Enhancement of Dye-sensitized Solar Cells Efficiency Using Graphene Quantum Dots as Photoanode

Jinmo Kim,[†] Bongsoo Lee,[‡] Young Jun Kim,[§] and Sung Won Hwang[¶,*]

[†]*Micro LED Research Center, Korea Photonics Technology Institute, Gwangju 500-779, South Korea*
[‡]*Department of Energy Systems Engineering, Chung Ang University, Seoul 06974, South Korea*
[§]*Department of Biomedical Chemistry, College of Biomedical & Health Science, Nanotechnology Research Center, Konkuk University, Chungju-si 27478, Republic of Korea*
[¶]*Department of Nano Science & Mechatronics Engineering, Nanotechnology Research Center, Konkuk University, Chungju-si 27478, Republic of Korea. *E-mail: swhwang@kku.ac.kr*
Received December 3, 2018, Accepted December 12, 2018, Published online December 26, 2018

Dye-sensitized solar cell (DSSC) is a candidate to substitute conventional photovoltaic devices due to efficiency, cost in comparison with silicon devices. In this report, graphene quantum dots have attracted considerable potential merit for the development of photo-electrodes of dye-sensitized photovoltaic cells. The incorporation of graphene quantum dots into DSSCs photo-electrodes induced lower recombination, enhanced electron transport, increased light scattering. The conventional semiconductor quantum dots usually has surface defect and instable. To overcome such limitations, we have developed a hydrothermal synthesis process fabricating graphene quantum dots (GQD) with strong visible range emission. The reduced GOs graphene oxide (RGO) underwent sonication, heating, filtering, and dialysis producing GQD. Various sizes of GQDs with circular shape determined using scanning electron microscopy, high-resolution transmission electron microscopy, Fourier transform infrared spectroscopy, X-ray photoelectron spectroscopy, and photoluminescence were successfully fabricated. In addition, the impedance nyquist plot, the electron transport resistance was smallest and the incident photo to charge carrier efficiency (IPCE) was the maximum when the size of graphene quantum dots (5 nm) was used. Thus, the GQD with unique optical and structural properties can be a very attractive candidate for dye-sensitized solar cells, optoelectronics, active layer of display, and bio-imaging devices.

Keywords: Graphene quantum dot, Graphene oxide, Reduced graphene oxide, Hydrothermal

Introduction

Recently, Quantum dot (QD) is a nanocrystal semiconductor, which changes energy band gap depending on its size and shape. The quantum mechanistic phenomenon of nano-sized semiconductor localizing electron movement provides energy state and optical characteristics.[1–3] The state of being confined excitations in semiconductor microstructure at nanoscale resulted in quantum confinement effect.[4,5] The density of states of QD is the same as the delta function but different from bulk materials. Therefore, QD emits almost the same light as the monochromatic light in a narrow wavelength region. Various research studies conducted to develop QD as a luminescence material for light-emitting diode (LED), because of its unique properties including high quality of color rendering, emission efficiency, color reproducibility, and QD size-dependent energy band gap and color. In addition, liquid processing of QD is cost effective and providing large information area that enables fabrication of information device. The QD fabricated by colloid synthesis has a 20–30 nm luminescence full width at half maximum (FWHM), which is at least one third of the other fluorescence system. In particular, CdSe and InP QD are suitable QD for display since they can emit any visible wavelength including trichromatic light by controlling the QD size.[6] In addition, nanocrystal QD is quite stable than organic luminescence material, which can be degraded by photochemical reaction. Therefore, colloidal QD has been developed for next generation light source of human sensibility since it has high efficiency of luminescence in visible wavelength region, narrow FWHM, and optical stability. However, the optical characteristics of colloidal QD can be degraded by high temperature and moisture. QD with Cd make it difficult to apply for optoelectronic device due to its toxicity and defect on surface. On the other hand, graphene quantum dot (GQD) has a large surface area, no defect and stable at high temperature, and capable of functionalization on the edge of GQD.[7,8] The unique structure of a sp^2-carbon domain and edge-functionalization of GQDs provides spontaneously ways to surface passivation and functional groups as well as tunable bandgap properties. Due to high surface to volume ratio GQDs are utilized in a wide range of applications including biological-, and optical-devices. GQDs are atomic level thickness, nano-

 © 2018 Korean Chemical Society, Seoul & Wiley-VCH Verlag GmbH & Co. KGaA, Weinheim

plate of sp^2 hybridization with conduction, which show size, and edge related electrical and optical characteristics.[9] Therefore, it is essential to be able to handle the size and edge state of GQD for its functionalization. Thus, the current study conducted to propose a high-quality GQD producing technique that can overcome limitations of conventional colloidal QD with analysis of structural and optical characteristics of various sizes of GQD. In this work, employed GQD with TiO_2 and searched for the best combination. GQD (approximately 5.0–10.0 nm) TiO_2 was synthesized. The synthesized devices were characterized by transmission electron microscopy (TEM), and impedance analysis. The photovoltaic performance of the GQD TiO_2/dye solar cell was evaluated from the power conversion efficiency, V_{oc} and J_{sc}.

Experimental

Recently, Graphene oxide (GO) were prepared from graphite powder by the Hummers method[10,11] with minor modification. The GO were deoxidized in a horizontal furnace at approximately 200–350°C for 2 h under Ar for reduced graphene oxide powder. About 0.05–0.5 g of graphene oxide power was oxidized by ultra-sonication in concentrated 15 mL H_2SO_4 and 40 mL HNO_3 for 10 h. 250 mL deionized water was used to dilute the mixture. It was filtered by a 200 nm membrane to neutralize. The reduced and purified 0.2 g GO powder was dissolved in 40 mL deionized water and NaOH was used to set the pH to 8. The aliquot was transferred to a nitrogen atmosphere furnace and heated at approximately 220–310°C for 6 h. After cooling to room temperature, the remaining powder was redispersed in 30 mL deionized water for 1 h under ultrasonication. Then, a brown solution was separated by filtering the suspension using a 200 nm membrane. Because some small graphene nanoparticles (< 50 nm) emitting weak blue luminescence are still remained in the colloidal solution, the brown solution was undergo dialysis (3500 Da) for 12 h, obtaining GQDs with strong fluorescence. The GQDs were extracted in different size using different dialysis bags of 1000–50 000 Da and a 20 nm membrane. The configuration of GQDs was determined by a transmission electron microscopy (200 kV; JEOL JEM-2100, Tokyo, Japan). In order to prepare the HRTEM/SEM and AFM samples the GQDs were suspended in deionized water, a drop of which was then put on a SiO-coated Cu grid (Tedpella, Inc.) and mica substrate, respectively. The topography and height of GQDs were determined at a tapping-mode of AFM (Park Sys., XE-100). The Fourier transform infrared spectroscopy (FTIR) spectrum were measured by a Nicolet iS5 FTIR (Thermo Fisher Scientific, Waltham, MA, USA) spectrometer with the KBr pellet method. X-ray photoelectron spectroscopy (XPS) was performed using a Thermo Scientific Escalab 250Xi (Waltham, MA, USA) with Al Kα X-ray radiation as the X-ray source for excitation. Binding energies were corrected using the C1s peak at 284.7 eV as the standard. PL spectra were evaluated at room temperature using a grating monochromator. The direct growth graphene was characterized using Raman spectroscopy (JY LabRam HR, 514.5 nm line of an Ar + laser, Kyoto, Japan). To manufacture dye-sensitized solar cells (DSSCs), a paste of the GQD TiO_2 was performed by mixing 3.0 g of GQD TiO_2 powders with a blend consisting of 10.0 g of α-tepinol, 1.5 g of cellulose, and 30 mL of ethanol, after sonication for 12 h at 1400 W cm^{-2}. A GQD TiO_2 composite was fabricated by coating onto an FTO conducting glass plate (approximately 25 ohm cm^{-2}, 85% transmittance) using a screen printing process. The film was performed by heating at 400°C for 60 min to remove the surface ingredient. For DSSCs manufacture, the prepared electrode was involved in a 3.0×10^{-4} M N719 dye solution at room temperature for 1 h, rinsed with ethanol and dried. A Pt coated FTO electrode was placed over the dye immersed GQD TiO_2 electrode, and the edges of the cell were sealed with a sealing tape. The redox electrolyte consisted of 0.7 mol KI, 0.07 mol I_2, and 0.7 mol 4-tert-butylpyridine as a solvent. The photocurrent voltage curves were used to calculate the V_{oc}, J_{sc}, FF, and power conversion efficiency of the GQD-TiO_2-DSSCs. I–V curves were measured under white light irradiation from a xenon lamp. The incident light intensity and cell area were 100 mW cm^{-2} and 0.5×0.5 cm^2, respectively. The AC-impedance measurements were employed with a potentiostat-galvanostat equipped with a electrochemical interface from IVIUM technique under constant light illumination of 100 mW cm^{-2}. EIS of the GQD DSSCs was employed under light illumination and open circuit voltage. The photoelectric properties were measured using a voltmeter (Model 2000; Keithley, Cleveland, OH, USA) with a shift load. A voltmeter above power breakdown and a lock-in amplifier were used. A 150 W illuminant Xenon lamp was utilized as a radiation source.

Results and Discussion

Figure 1 presents a scheme of GQD fabrication process. The reduced graphene oxide (RGO) was produced by graphene oxide (GO) fabrication with chemical acid treatment of graphite followed by reduction process using thermal treatment. GQD was extracted by repeated tip sonication and thermal treatment followed by filtering. The oxidation and reduction processes during fabrication of GO and RGO can determine the size and shape of GQD.

Figure 2 presents typical scanning electron microscopy (SEM) and atomic force microscopy (AFM) images of the graphene flakes and GQDs. The diameters of GQDs are usually approximately 5–40 nm. Firstly, the GO was made from the oxidation of graphite followed by thermal reduction of GO resulting in RGO. Then the GQD was made from the RGO. Before the hydrothermal application, the graphite were oxidized using concentrated H_2SO_4 and HNO_3. Finally, the GQDs were produced by a dialysis. The

 © 2018 Korean Chemical Society, Seoul & Wiley-VCH Verlag GmbH & Co. KGaA, Weinheim

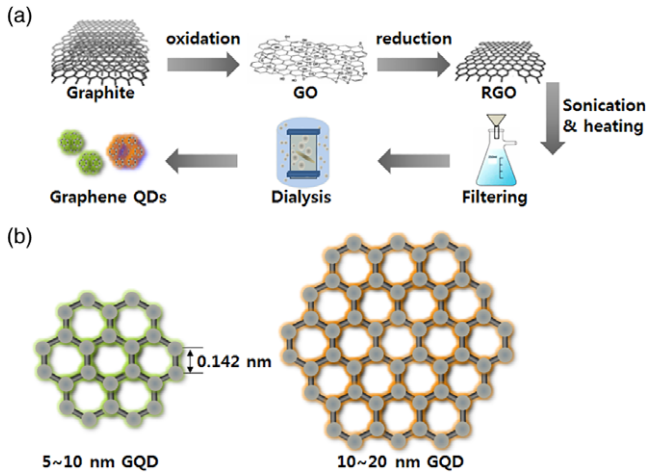

Figure 1. Scheme of graphene quantum dot (GQD) fabrication process by step (a) and the sizes of GQD (b).

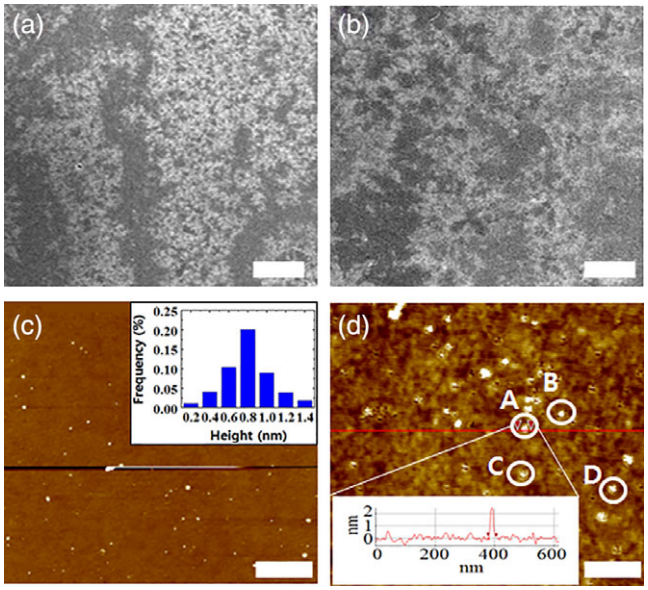

Figure 2. A scanning electron microscopic (SEM) images of the graphene flakes and graphene quantum dots (GQDs) before filtering, the scale bar indicates 10 μm (a), and after dialysis with a dialysis bag of 3500 Da, the scale bar indicates 5 μm (b). The typical atomic force microscopic (AFM) image of the GQDs, the scale bar indicates 1 μm (c) the inset indicates height distribution of a typical GQD and zoom in image with randomly chosen GQDs A, B, C, and D, the scale bar indicates 100 nm (d). The inset indicates the line profile of a typical GQD.

graphene flake had an irregular size distribution before filtering (Figure 2(a)), and after extracting with a dialysis bag of 3500 Da (Figure 2(b)). Figure 2(c) is the typical AFM image of the GQDs, The inset distribution curve indicates that the height of the GQD is approximately 0.8 nm, in excellent correspondence with the thickness of monolayer graphene quantum dot. Figure 2(d) is the AFM image of the GQDs after drying 90 min at room temperature and zoom in image of GQD. The GQDs present circular shape. A, B, C, and D are randomly selected GQDs. The

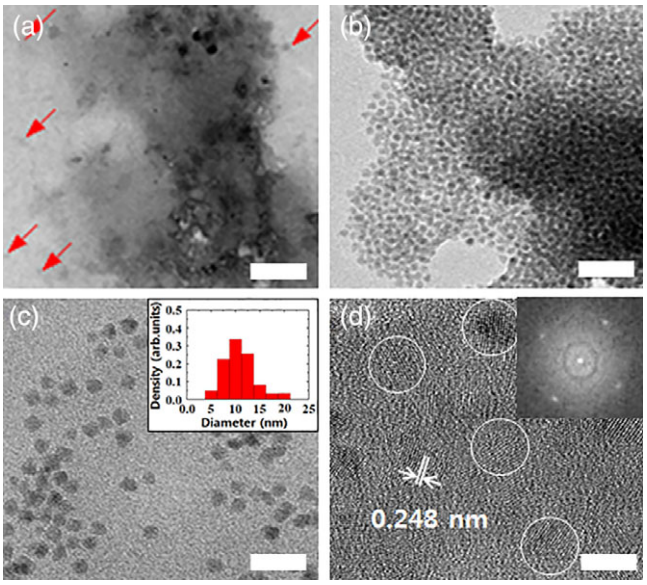

Figure 3. A transmission electron microscopic (TEM) image of GQDs (red arrows), the scale bar indicates 200 nm (a), a high-resolution TEM image, the scale bar indicates 100 nm (b), a high-resolution TEM image of the irregular shape of GQDs, the scale bar indicates 50 nm (c), and a high-resolution TEM image (white circle) of GQDs, the scale bar indicates 5 nm (d).

diameters of GQD of A, B, C, and D were 12, 15, 21, and 22 nm, respectively. The average height was 1.4 nm in accordance with the average height of the GQDs evaluated by the transmission electron microscopy (TEM). To determine the growth property of GQD, characterization of AFM and TEM on the shape and size of the GQDs has been carried out. The white protrusion cannot be defined as a single QD since the GQD aggregates due to the van der Waals interaction.

Figure 3 presents high-resolution TEM image of GQDs. The uniform coating is one of the merit of our technique compared to the other GQDs fabrication procedure. Figure 3(a) presents a typical TEM image of GQDs (red arrows). Figure 3(b) clearly indicates high-resolution TEM (HR-TEM) images of GQDs. We have previously reported that[9] the photoluminescence of GQD is associated with the shape and size of GQDs. The average diameters of GQDs analyzed by the TEM images are estimated to be 10.03 ± 0.05 and 12.21 ± 0.05 nm, respectively, as shown in Figure 3(c). The HR-TEM images of the irregular shape of GQDs (Figure 3(d)) present the existence of lattice spacing of 0.248 nm, and number of graphene layers (approximately 1–3) in the GQDs, which correspond to the space of the basal flat surface of the hexagonal structure.[12] The inset image indicates that the electron diffraction pattern by transmission electron microscopy in Figure 3(d) confirm the high lattice quality of the monolayer graphene. The image indicates the circular shapes of the GQDs. It should be noted that the 0.248 nm of lattice distance at the basal plane of GQDs is larger than that of graphite. It is plausible that the functional groups present at the edges lead to the

 © 2018 Korean Chemical Society, Seoul & Wiley-VCH Verlag GmbH & Co. KGaA, Weinheim

increase in the spacing of graphite basal flat surface. It is well known that the edge of GQDs has COOH group with oxygen and mix zigzag and armchair structures.[9] Recent, study[13–15] indicates that the chemical bond and free energy at the edge of GQD are higher than those of the center. On the other hand, the core of the GQDs characterized by no defect single crystal with hexagonal structure can be important for uniform wavelength during luminescence of quantum confinement effect (QCE) and maximized luminescence intensity. In addition, recent study[16–19] indicates that improved mechanical and electrical properties can be achieved by selective electro-deposition of metal on graphene defects.

Figure 4 presents X-ray photoelectron spectroscopy (XPS) spectrum and Fourier transform infrared (FTIR) spectroscopy spectrum of GQDs. The XPS and FTIR to determine the compositions and characterization using peak analysis. Figure 4(a) presents a typical XPS high-resolution spectrum of C1s peaks in the GQDs. The high-resolution spectra of deconvolution C1s peaks of C=C/C–C (283.8 eV), C═O (286.9 eV), and C—O (284.9 eV), respectively. The high-resolution spectrum of O1s confirmed the existence of C═O (530.1 eV), C-OH (532.1 eV), and O=C–OH (534.9 eV) peaks (Figure 4(b)). As shown in the FTIR (Figure 4(c)), the absorption spectrum centered at 1403 and 1593 cm^{-1} are assigned to the symmetric and asymmetric vibrations mode of COO–, respectively. The absorption spectrum centered at 3429 cm^{-1} is assigned to O—H stretching vibration mode. It should be presented that the GQDs indicate no absorption bands of C—H and C–O–C, logically present that they have incorporation defects and edge-functionalization of carboxyl group.[20–24] The oxygen termination make GQDs soluble in aqueous process. Figure 4(d) presents a typical XPS spectrum of the GQDs. The GQDs are consisted of C, O, Na and H. The XPS spectrum of C1s bands could be deconvoluted into three peaks.

Figure 5 shows photoluminescence (PL) spectrum of GQDs and graphene flakes in deionized water excited at 325 nm. The central wavelength and the behavior of the PL spectra are strongly related to the diameter of GQDs and graphene flakes.

The inset of Figure 5(a) presents blue luminescence of various sizes of GQDs and graphene flakes. Several strong peaks present in the spectrum may be because of the photoluminescence properties of graphene nanostructures (*e.g.,* graphene quantum dot, graphene nano-ribbon, nanotube, graphene nanowire) in deionized water as shown in Figure 4(a). Our previous studies also confirmed[9] that the absorption spectra, photoluminescence, and EELS characteristics can be altered. It has been reported that oxygen-functional groups may exist at the edge structures of GQDs after the hydrothermal method in the manufacture processes of GQDs, leading to the PL behaviors of GQDs.[25–27] Previous research studies have suggested that the band gap of GQDs in the diameters of approximately 5–35 nm are less than approximately 1.0 eV.[28,29] Current study indicates that graphene nanostructures can control 1–3 eV of bandgap by its shape and size and that the fine bandgap can also be determined by surface functionalization, inorganic quantum dot and hybrid structure. Previous theoretical study[30,31] supports such notion. The Figure 5(b) presents blue luminescence of various sizes of GQDs. The visible PL in a graphene has been suggested to identify minimization of thermal equilibrium. It is probably due to the electron phonon scattering from high-power light source.[32] In addition the light scattering can be caused by excited state relaxation

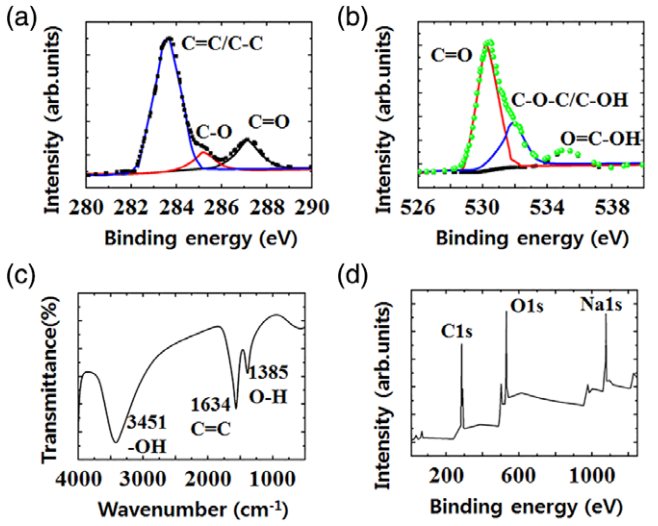

Figure 4. (a) X-ray photoelectron spectroscopy high-resolution spectrum of C1s peaks in the GQDs. (b) X-ray photoelectron spectroscopy high-resolution spectrum of O1s core levels in the GQDs. (c) Fourier transform infrared spectroscopy spectrum of the GQDs. (d) X-ray photoelectron spectroscopy survey spectrum of the GQDs.

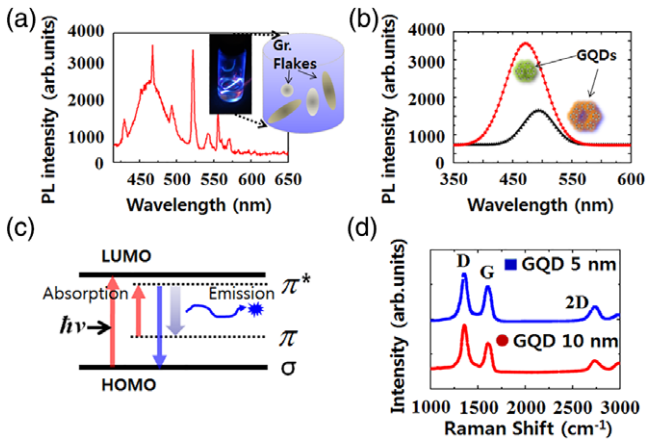

Figure 5. A photoluminescence (PL) spectra of graphene quantum dot (GQD) in deionized water excited at 325 nm. (a) The image shows visible range luminescence of various sizes of graphene flakes and GQDs. (b) Size-dependent PL spectra for GQDs of 5.3 and 10.1 nm average diameters and proposed energy band diagram of GQD (c). (d) Size-dependent Raman spectra of GQDs.

 © 2018 Korean Chemical Society, Seoul & Wiley-VCH Verlag GmbH & Co. KGaA, Weinheim

and by adding a dopant electrically.[33] Optical properties of graphene determined by photoluminescence indicate that the monolayer of graphene had higher amplification of PL than that of multiple layers. Structurally, when graphene plasmon hybridizes with nanostructure, optical amplification of PL can be achieved by the graphene plasmon.[34–36]

PL spectra of various size of graphene flake and GQDs in Figure 5 suggest the importance of the distribution of size and shape. The current study clearly indicates that the process of GQDs fabrication provides an effective technique controlling the GQDs diameter within a limited range without alteration of the optical properties of the GQDs. The energy band diagram of the GQD is suggested as presented in Figure 5(c). The covalent σ bond is formed from the neighboring carbon atoms resulted in the formation of GQD. The π and π * bonds are generated by the delocalization of π electrons. The functional groups with oxygen at the surface of the GQD can cause the oxygen surface state between filled band and unfilled band. Figure 5(d) shows

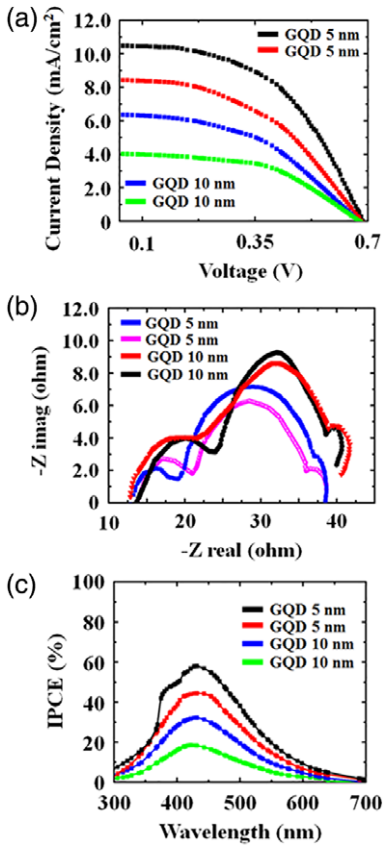

Figure 6. (a) presents the photocurrent voltage behavior of the DSSCs assemble a photo-anode and the 5.0, and 10.0 nm GQDs. The device thickness was in the scope of 9.0-11.0 mm and the cell area was fixed with sizes of 5.0 × 5.0 mm^2. A DSSCs assembled with TiO_2 photo-anode had a V_{oc} of 0.71 V and a J_{sc} of 8.14 $mAcm^{-2}$ at an photon intensity of 100 mW/cm^2. The energy conversion efficiency was 4.23% for the TiO_2 photo-anode, but increased to 6.17% in the DSSC made from 5 nm GQD-TiO_2, with a J_{sc} of 10.39 $mAcm^{-2}$ and a V_{oc} of 0.69 V.

the Raman spectra of GQDs. Two main modes, D and G, a 2D band at 2748 cm^{-1} assign to a vibration mode, and a interaction of the D and G bands arise from a band 2917 cm^{-1} as a result from lattice vibrations. The D band is described in the existence of defects, implying that the resulting graphene layers have considerable defects.

Figure 6(a) presents the photocurrent voltage behavior of the DSSCs assemble a photo-anode and the 5.0, and 10.0 nm GQDs. The device thickness was in the scope of 9.0–11.0 mm and the cell area was fixed with sizes of 5.0 × 5.0 mm^2. A DSSCs assembled with TiO_2 photo-anode had a V_{oc} of 0.71 V and a J_{sc} of 8.14 $mAcm^{-2}$ at an photon intensity of 100 mW/cm^2. The energy conversion efficiency was 4.23% for the TiO_2 photo-anode, but increased to 6.17% in the DSSC made from 5 nm GQD-TiO_2, with a J_{sc} of 10.39 mA cm^{-2} and a V_{oc} of 0.69 V.

Figure 6(b) shows impedance analysis of GQDs-DSSCs, normally, the electrochemical impedance spectra of the DSSC presents three semicircles in the frequency range of 0.1–100 kHz. The second frequency semicircle (R_{ct2}) is related to the electron transport at the GQDs TiO_2/dye/electrolyte interface. The second semicircle reduced considerably attributable to the effects of the dopant of graphene. The TiO_2 DSSC and 10 nm-GQDs-DSSCs occurred to have a higher electron transport resistance in the flow of electric charge through the device than that of the 5 nm GQDs-DSSCs, remarkably, R_{ct2} was reduced in the device with the 5 nm GQDs-DSSCs compared with that of the TiO_2 control sample. It is conspicuous that the carrier flow from the valence band of the dye to the electrode via the HOMO of GQDs. Figure 6(c) shows IPCE curves of GQDs-DSSCs, the DSSCs that response to the wavelength of visible range photon were obtained in the 300–700 nm.[37–41] The dye that reacted at a 400–500 nm had the maximum incident photo to charge carrier efficiency (IPCE), which is equivalent to the absorption band of dye due to π* metal to ligand carrier transfer. The quantum number of the GQDs-DSSCs was about 38%, but this was increased to about 59.6% in the 5 nm GQDs-DSSCs. Consequentially, the quantum efficiency was increased to approximately 56.8%, which confirmed that the GQD photo-anode induced more the number of photons.

Conclusion

We developed a mass hydrothermal synthesis carbonization process to synthesize GQDs. Size controllable monolayer GQDs (4.8 ~ 22.1 ± 0.5 nm) with fluorescent have been accomplished via membrane filtration. The current study developed a hydrothermal synthesis process for converting GO to GQDs with sensitive visible range emission. Various sizes of GQDs were successfully fabricated and their structures were determined by SEM, HRTEM, XPS, FTIR, and PL. The impedance nyquist plot, the electron transport resistance was smallest and the incident photo to charge carrier efficiency (IPCE) was the maximum when the size

 © 2018 Korean Chemical Society, Seoul & Wiley-VCH Verlag GmbH & Co. KGaA, Weinheim

of graphene quantum dots (5 nm) was used. The conversion efficiency was increased by the application of graphene quantum dots photo-anode layers in the DSSCs to approximately 6.17% for graphene quantum dots (5 nm) and cell area (5.0×5.0 mm^2). Thus, the GQD with unique optical and structural properties is a promising candidate substituting the conventional semiconductor quantum dots. The photoluminescence and Raman spectra of GQDs have been shown to be effective for sensors, LED, and bio-imaging.

Acknowledgments. This work was supported by Rural Development Administration, Republic of Korea (PJ011885).

References

1. C. d. Donegá, *Chem. Soc. Rev.* **2011**, *40*, 1512.
2. A. P. Alivisatos, *J. Phys. Chem.* **1996**, *100*, 13226.
3. R. Rossetti, L. Brus, *J. Phys. Chem.* **1982**, *86*, 4470.
4. S. V. Gaponenko, *Cambridge University Press*. **2010**, p. 97.
5. V. I. Klimov, *Annu. Rev. Phys. Chem.* **2007**, *58*, 635.
6. Y. Zhu, S. Murali, W. Cai, X. Li, J. W. Suk, J. R. Potts, R. S. Ruoff, *Adv. Mater* **2010**, *22*, 3906.
7. X. Wu, F. Tian, W. Wang, J. Chen, M. Wu, J. X. Zhao, *J. Mater. Chem. C* **2013**, *31*, 4676.
8. F. Bonaccorso, Z. Sun, T. Hasan, A. C. Ferrari, *Nat. Photo.* **2010**, *4*, 611.
9. S. Kim, S. W. Hwang, M. K. Kim, D. Y. Shin, D. H. Shin, C. O. Kim, G. Ko, *ACS Nano* **2012**, *6*, 8203.
10. Y. Xu, H. Bai, G. Lu, C. Li, G. Shi, *J. Am. Chem. Soc.* **2008**, *130*, 5856.
11. D. Pan, S. Wang, B. Zhao, M. Wu, H. Zhang, Y. Wang, Z. Jiao, *Chem. Mater.* **2009**, *21*, 3136.
12. L. B. Biedermann, M. L. Bolen, M. A. Capano, D. Zemlyanov, R. G. Reifenberger, *Phys. Rev. B* **2009**, *79*, 125411.
13. D. Pan, Z. Zhang, Li, M. Wu, *Adv. Mater* **2010**, *22*, 734.
14. J. Peng, W. Gao, B. K. Gupta, Z. Liu, R. Romero-Aburto, L. Ge, S. A. Vithayathil, *Nano Lett.* **2012**, *12*, 844.
15. Z. Z. Zhang, K. Chang, F. M. Peeters, *Phys. Rev. B* **2008**, *77*, 235411.
16. A. D. Güçlü, P. Potasz, P. Hawrylak, *Phys. Rev. B* **2010**, *82*, 155445.
17. W. T. Liu, S. W. Wu, P. J. Schuck, M. Salmeron, Y. R. Shen, F. Wang, *Phys. Rev. B* **2010**, *82*, 081408.
18. C. H. Lui, K. F. Mak, J. Shan, T. F. Heinz, *Phys. Rev. L.* **2010**, *105*, 127404.
19. C. F. Chen, C. H. Park, B. W. Boudouris, J. Horng, B. Geng, C. Girit, F. Wang, *Nature* **2011**, *471*, 617.
20. Y. Li, H. Shu, X. Niu, J. Wang, *J. Phys. Chem. C* **2015**, *119*, 24950.
21. L. Tang, R. Ji, X. Cao, J. Lin, H. Jiang, X. Li, S. P. Lau, *ACS Nano* **2012**, *6*, 5102.
22. S. Zhu, J. Zhang, C. Qiao, S. Tang, Y. Li, W. Yuan, H. Gao, *Chem. Commun.* **2011**, *47*, 6858.
23. Y. Dong, J. Shao, C. Chen, H. Li, R. Wang, Y. Chi, G. Chen, *Carbon* **2012**, *50*, 4738.
24. G. Chen, Z. Zhuo, K. Ni, N. Y. Kim, Y. Zhao, Z. Chen, X. Wu, *Small* **2015**, *11*, 5296.
25. R. Liu, D. Wu, X. Feng, K. Müllen, *J. Am. Chem. Soc.* **2011**, *133*, 15221.
26. K. L. Schroeder, R. V. Goreham, T. Nann, *Pharm. Res.* **2016**, *33*, 2337.
27. Q. Zhuang, Y. Wang, Y. Ni, *Luminescence* **2016**, *31*, 746.
28. T. Gao, X. Wang, L. Y. Yang, H. He, X. X. Ba, J. Zhao, Y. Liu, *ACS Appl. Mater. Inter.* **2017**, *9*, 24846.
29. R. Gokhale, P. Singh, *Part. Syst. Charact.* **2014**, *31*, 433.
30. C. Wu, C. Wang, T. Han, X. Zhou, S. Guo, J. Zhang, *Adv. Healthc. Mater.* **2013**, *2*, 1613.
31. J. Kim, J. S. Suh, *ACS Nano* **2014**, *8*, 4190.
32. S. Bian, C. Shen, Y. Qian, J. Liu, F. Xi, X. Dong, *Sen. Actuators B: Chem.* **2017**, *242*, 231.
33. T. Alizadeh, M. Shokri, Y. Hanifehpour, S. W. Joo, *J. Environ. Anal. Chem.* **2016**, *96*, 763.
34. V. V. Chaban, O. V. Prezhdo, *Nanoscale* **2015**, *7*, 17055.
35. T. Yoon, J. H. Kim, J. H. Choi, D. Y. Jung, I. J. Park, S. Y. Choi, T. S. Kim, *ACS Nano* **2016**, *10*, 1539.
36. S. W. Hwang, D. H. Shin, C. O. Kim, S. H. Hong, M. C. Kim, J. Kim, G. Kim, *Phys. Rev. L.* **2010**, *105*, 127403.
37. Q. Shen, T. Sato, M. Hashimoto, C. Chen, T. Toyoda, *Thin Solid Films* **2006**, *499*, 299.
38. H. Hu, X. Wang, J. Wang, F. Liu, M. Zhang, *Appl. Surf. Sci.* **2011**, *257*, 2637.
39. J. Wu, X. Shen, L. Jiang, K. Wang, K. Chen, *Appl. Surf. Sci.* **2012**, *256*, 2826.
40. X. Wang, L. Zhi, K. Mullen, *Nano Lett.* **2008**, *8*, 323.
41. S. Stankovich, D. A. Dikin, R. D. Piner, K. A. Kohlhaas, A. Kleinhammes, Y. Jia, Y. Wu, S. B. T. Nguyen, R. S. Ruoff, *Carbon* **2007**, *45*, 1.

 © 2018 Korean Chemical Society, Seoul & Wiley-VCH Verlag GmbH & Co. KGaA, Weinheim